Design and Performance Analysis of THz Wireless Communication Systems for Chip-to-Chip and Personal Area Networks Applications

Changhwan Yi, Dongkyo Kim, *Graduate Student Member, IEEE*, Sourabh Solanki, *Member, IEEE*, Jae-Hong Kwon, *Member, IEEE*, Moonil Kim, *Senior Member, IEEE*, Sanggeun Jeon, *Member, IEEE*, Young-Chai Ko, *Senior Member, IEEE*, and Inkyu Lee, *Fellow, IEEE*

***Abstract*— Terahertz (THz) communication is a promising technique for chip-to-chip communication and wireless personal area networks. In this paper, we present an experimental study and design to realize such THz communication systems. We develop two different chip sets for on-off-keying (OOK) modulation based THz transceivers which include carrier generators, modulators, THz amplifiers, and baseband amplifiers. Specifically, the first chip set integrates the circuit blocks for the OOK modulation without the THz amplifier for short-range communication. In addition, the second chip set design includes the THz amplifier modules to extend the coverage of transmission. For these two chip sets, we experimentally demonstrate the feasibility of the wireless communication at THz frequency bands and assess performance using the bit error rate (BER) analysis. We estimate the BER by calculating the signal-to-noise ratio (SNR) based on the eye diagram and compare with actual BER measurements and Monte Carlo simulations. We also address the impact of the distance, the transmit power, and the data rate for the proposed THz transceivers based on the link budget analysis, and confirm the accuracy of the derived BER expression.**

***Index Terms*— THz communications, THz transceivers, on-off keying, integrated circuit.**

Manuscript received June 15, 2020; revised November 16, 2020 and February 17, 2021; accepted March 1, 2021. Date of publication April 8, 2021; date of current version May 18, 2021. This work was supported in part by the Institute of Information & Communications Technology Planning & Evaluation (IITP) funded by the Ministry of Science and ICT (MSIT), Korea Government (Development of ultra-wideband terahertz CW spectroscopic imaging systems based on electronic devices) under Grant 2021-0-00185 and in part by the National Research Foundation (NRF) through the Ministry of Science, ICT, and Future Planning (MSIP), Korea Government, under Grant NRF-2020R1A4A1019628 and Grant 2017R1A2B3012316. This article was presented in part at the International Conference on ICT Convergence (ICTC), Jeju Island, South Korea. *(Corresponding author: Inkyu Lee.)*

Changhwan Yi, Jae-Hong Kwon, Moonil Kim, Sanggeun Jeon, Young-Chai Ko, and Inkyu Lee are with the School of Electrical Engineering, Korea University, Seoul 02841, South Korea (e-mail: shuma394@korea.ac.kr; hugokwon@korea.ac.kr; mkim@korea.ac.kr; sgjeon@korea.ac.kr; koyc@korea.ac.kr; inkyu@korea.ac.kr).

Dongkyo Kim was with the School of Electrical Engineering, Korea University, Seoul 02841, South Korea. He is now with Samsung Electronics, Suwon 16677, South Korea (e-mail: dongkyo@korea.ac.kr).

Sourabh Solanki was with the School of Electrical Engineering, Korea University, Seoul 02841, South Korea. He is now with the Interdisciplinary Centre for Security, Reliability, and Trust (SnT), University of Luxembourg, 4365 Luxembourg, Luxembourg (e-mail: sourabhsolanki@ieee.org).

Color versions of one or more figures in this article are available at https://doi.org/10.1109/JSAC.2021.3071849.

Digital Object Identifier 10.1109/JSAC.2021.3071849

I. Introduction

FOR the past few decades, the bandwidth required for wireless communication systems has been continuously increasing to satisfy high demands of various data hungry applications and services. Such a trend is rightly predicted by Edholm's law [2] which states that the bandwidth and the data rates double in about every 18 months. Following a similar trend, the global mobile data traffic, which currently exceeds 38 exabytes per month, is anticipated to reach 160 exabytes per month by the year 2025 [3]. Since the capacity of wireless links in existing networks is approaching the fundamental limit, it becomes more important to achieve higher data rate by acquiring larger bandwidth. Consequently, the research community has been exploring the possibilities of shifting to higher frequency bands such as millimeter wave (mmWave) or terahertz (THz) frequencies [4].

Current 5^{th} Generation (5G) systems plan to adopt the mmWave band with the bandwidth of 7-9 GHz. To prepare for beyond 5G systems, the THz frequency band whose frequency ranges from 0.1 THz to 10 THz starts to garner large attentions due to its virtually unlimited bandwidth. The THz communication is expected to support over 1 Tbps with moderate and viable spectral efficiency, which can revolutionize the next 6G wireless networks [5].

In contrast to mmWave technologies where significant design efforts have already been made, the research for the development of THz communication is still in its infancy. Recently, a THz interest group (IGthz) has been formed under the IEEE 802.15 wireless personal area networks (WPAN) [6] to focus on the THz communication and their network related applications. WPANs are self-organizing networks which can provide high data rates for short-range communications, i.e., Bluetooth, Zigbee, etc. As such, the evolution of internet-of-things (IoT) would require high speed interconnection among several devices such as virtual reality headset, smart watches, etc.

In fact, mmWave and optical wireless communication (OWC) can also offer higher data rates compared with traditional microwave communications. However, there exist certain limitations to these two technologies that inspire the

application of the THz technology. Although the mmWave band can provide a larger bandwidth compared with the sub-6 GHz in 5G, the usable bandwidth in the mmWave band is confined to 7-9 GHz which imposes a limit on the maximum data rates [7]. For instance, in 60 GHz band, the work in [8] has shown the achievable data rates of 50 Gbps. More recently, the authors in [9] have presented the data rates of up to 15 Gbps in 28 GHz band. However, it is important to note that all these works employed higher order modulation techniques or multiple antennas, which consume more power. In [10], the authors have reported the data rate of 3 Gbps at 60 GHz by adopting a simple low-power on-off keying based modulation scheme. Nevertheless, to obtain the data rate of over 100 Gbps, it is required to achieve the spectral efficiency of at least 12 bps/Hz which is extremely difficult to realize in the mmWave band using the conventional transceiver architectures [4].

Also, OWC systems possess huge bandwidth that can potentially offer high-data rates. However, the OWC systems suffer from a low power transmission budget due to skin safety regulations [11]. Further, the optical receiver in OWC is susceptible to background disturbances primarily from the shot noise induced by the ambient light sources. In OWC systems, visible light communication (VLC) is appropriate for the indoor and short range applications due to safety issues. To achieve high data rates in VLC systems, the transmitter and receiver are needed to be aligned to establish line-of-sight (LoS) links, which becomes challenging when users are mobile. Alternatively, a wide field-of-view is needed to capture sufficient optical power leading to large receiver aperture [12]. In contrast, THz communication allows the non-LoS propagation which can be exploited in the absence of LoS links [13]. Among recent works in VLC, the authors in [14] reported the maximum achievable data rate of 7.4 Gbps. Also, the work [15] emphasized that the achievable throughput in practical VLC is still several orders below than what had been claimed by various experiments. This work demonstrated a throughput of 80 kbps at a distance of two meters.

Due to these limitations of mmWave and OWC systems, the THz communications are considered as a promising solution to offer ultra high data rates in WPAN. In addition, for chip-to-chip communication applications, THz communication can be exploited to complement traditional bus-based architectures by establishing high speed wireless interconnects. One of key challenges to make THz transmission a reality is efficient generation, modulation, and detection of THz waves.

Recently, many research works have addressed various aspects of the THz communications. For instance, to characterize the propagation of THz waves, various studies and experimental demonstrations have been performed for outdoor [16]–[19], indoor [20]–[22], and nanoscale [23]–[25] channel environments. Also, since it is exceedingly difficult to generate and detect the THz waves, several efforts have been made in the literature to explore device based solutions [26]–[30]. In particular, the use of graphene based nano-antennas was proposed in [26] to enable electromagnetic communications in nano-networks. The work [27] reviewed the role of photonic technologies for the development of THz communication systems. A study in [28] discussed the prospects of the diode technique for THz and sub-mmWave systems. Also, the operation of indium phosphide (InP) heterogeneous bipolar transistors was studied in [29] for THz frequencies. In [30], the authors comprehensively reviewed the advancements of THz integrated electronic and hybrid electronic-photonic systems and their applications in communication.

For THz frequencies, advanced modulation schemes such as quadrature amplitude modulation (QAM) require architectures that are still too complex at the current stage of circuit developments. Therefore, ultra high data rate communication systems are best realized by employing simple modulation schemes with low spectral efficiency such as on-off-keying (OOK), and taking advantage of the wide available frequency bandwidth. In recent years, several THz transceivers operating at the frequency above 200 GHz have been implemented for the OOK modulation [31]–[33]. A 260 GHz 4th-harmonic based OOK transceiver [31] achieved 6 Gbps data transmission at the distance of 4 cm. A 3rd-harmonic based 210 GHz transceiver [32] showed 10.7 Gbps data transmission with 1 cm distance. In [33], a 10 Gbps wireless link was demonstrated by a fully integrated 210 GHz transceiver including an on-chip 2×2 antenna array. However, these transceivers presented only a demodulated spectrum [31], [33] or an eye diagram [32], and no further detailed experiment and analysis of the data transmission were provided. Moreover, the transmission distance and the data rate reported to these works were limited to 4 cm and 10.7 Gbps, respectively. In essence, to support higher data rates and longer transmission distance, more efficient chip design techniques and their comprehensive performance evaluation for the OOK modulation are necessary.

In this paper, we present an experimental framework of THz communications for their potential applications[1] in wireless chip-to-chip [35] and PAN. The main goal of our paper is to demonstrate the feasibility of THz communication implementation with efficient chip designs. Also, we provide a link budget analysis and extensive performance measurement results such as data rate and bit error rate (BER) which allow us to analyze design parameters for optimizing performance. In this work, we develop two different chip sets of THz OOK transceivers, which include different types of THz carrier generators, OOK modulators, THz amplifiers, and baseband amplifiers. Most of the previously reported OOK transceivers employ complex harmonic-based carrier generators and they suffer from low spectral purity and large system size [31], [32]. Furthermore, the results are not suitable for various analysis, because the output power of the transceivers is fixed. On the other hand, the proposed circuit blocks in this work operate based on fundamental mode carriers, leading to high spectral purity and simple system architecture. Moreover, THz amplifier waveguide modules are included as a transceiver component to increase the wireless link distance demonstrating

[1]The chip-to-chip communication is usually aimed at a typical distance of a few centimeters [31], [33]. In contrast, for PAN, the communication distance can vary from tens of centimeters to a few meters [34]. It is worth highlighting that our proposed chip designs can support the transmission range suited for both these applications, as we shall observe later in Section VI.

the feasibility of utilizing waveguide modules in THz systems for the first time.

The first transceiver chip set (TRX1) fully integrates the circuit blocks for OOK modulation except for a THz amplifier to verify a short-range communication capability with various carrier frequency and distance. In contrast, the second transceiver chip set (TRX2) incorporates an amplifier waveguide module to extend the communication distance. This transceiver is built as a block of modules, allowing the output power or antenna gain to be flexibly adjusted for better performance analysis. With these two transceiver chip sets, the wireless data transmission is experimentally demonstrated and analyzed in detail with various distance, data rate, carrier frequency, and transmit power. Also, we derive the BER estimate and confirm the accuracy compared with actual BER measurements.

The rest of the paper is organized as follows: Section II explains the channel model and the link budget of the THz communication system. The general architecture and experimental setup of THz OOK transceivers are presented in Section III. The detailed design of TRX1 and TRX2 are described in Sections IV and V, respectively. In Section VI, the performance results are illustrated and finally, in Section VII, the conclusions are drawn and future research directions are provided.

II. THz Channel Model and Link Budget

A. THz Propagation Characteristics

In this section, we describe the propagation characteristics of THz wireless channels. A total loss of the received signal is composed of the free space path loss (FSPL) and the atmospheric absorption loss (AAL). Particularly, it has been known that the amount of absorption by oxygen (O_2) and water vapour (H_2O) is large in the THz channel. As a result, WPAN standard sets the THz bandwidth range from 220 GHz to 320 GHz [36]. Denoting d as the distance between a transmitter and a receiver and f as the carrier frequency, the total loss L_p is generally expressed as [37]

$$L_p(d,f) = \left(\frac{c}{4\pi f d}\right)^2 e^{\alpha_{\mathrm{AAL}}(f)d}, \tag{1}$$

where the first and second term account for the FSPL and the AAL, respectively, c represents the speed of light, and $\alpha_{\mathrm{AAL}}(f)$ indicates the AAL coefficient.

We can obtain $\alpha_{\mathrm{AAL}}(f)$ from the measurement data in international telecommunication union-radio (ITU-R) recommendation [38]. The AAL in a decibel unit linearly increases with the distance, while the FSPL in a decibel unit logarithmically grows with the distance. Hence the effect of the AAL becomes dominant in the long-distance outdoor communication. On the contrary, for the case of short-distance applications which THz communications are normally focused on, the AAL can be neglected. For instance, the value of α_{AAL} is measured as 2.23 dB/km at 220 GHz and 11.72 dB/km at 320 GHz, which means that the AAL from 220 GHz to 320 GHz is much smaller than 1 dB in tens of meters.

Therefore, in this paper, we consider a log-distance path loss model without the consideration of the AAL effect as [39]

$$L_p(d) = L_p(d_0)\left(\frac{d}{d_0}\right)^{\gamma}, \tag{2}$$

where d_0 and γ are the reference distance and the path loss exponent, respectively. The path loss exponent γ is normally known to be larger than 2 in outdoor environments, while there are some experimental results showing that the path loss exponent can be less than 2 in short-distance indoor communication [40].

B. Link Budget

To demonstrate the feasibility of a THz wireless communication link, it is necessary to compute the link budget and analyze the relationship between the transmit power, the BER, the distance, and other design parameters. Defining R_s and B_w as the data rate and the channel bandwidth, respectively, the received signal-to-noise ratio (SNR) of a wireless link is obtained as [41]

$$\mathrm{SNR} = \frac{P_t G_t G_r B_w}{N_o L_{Rx} L_p R_s}, \tag{3}$$

where P_t, G_t, G_r, N_o, and L_{Rx} represent the transmit power, the transmit antenna gain, the receive antenna gain, the noise power of a receiver, and the receiver implementation loss, respectively. Here, the input noise power N_o is given by

$$N_o = kT_0 B_w F, \tag{4}$$

where k, T_0, and F stand for the Boltzmann's constant $\left(k = 1.381 \times 10^{-23}\ \mathrm{Ws/K}\right)$, the receiver noise temperature in Kelvin, and the noise figure, respectively.

Substituting (2) into (3), we can express

$$R_s = \frac{A}{\mathrm{SNR}}\frac{P_t}{d^{\gamma}}, \tag{5}$$

where $A = \frac{G_t G_r d_0^{\gamma}}{kT_0 F L_{Rx} L_p(d_0)}$ is a constant related to a THz transceiver design and the reference path loss. From (5), we can obtain the relationship between the transmit power, the distance, the received SNR (i.e. BER), and the data rate.

III. Integrated THz OOK Transmitter and Receiver

In this section, we describe the general architecture of OOK based transceiver and present the details of an experimental framework for the wireless transmission at THz frequencies.

A. General Architecture

The OOK transmitter generally consists of a THz carrier generator, an OOK modulator and a power amplifier. For a THz carrier generator, an external amplifier multiplier chain (AMC) module fed by a low-frequency signal generator is commonly employed. On the other hand, to achieve a higher integration level and lower power consumption, an on-chip integrated voltage-controlled oscillator (VCO) can be used for the THz carrier generation. For the OOK modulation, the THz carrier generator is followed by a switching type

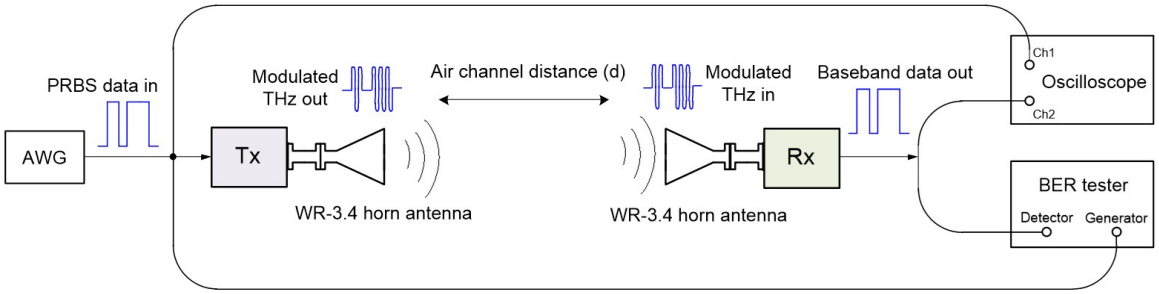

Fig. 1. Experiment setup for wireless data transmission of the THz OOK transceiver chip sets.

modulator, which can be implemented in either active or passive topologies. Finally, the modulated signal is amplified by a THz amplifier before transmission. The power amplifier can be integrated on-chip with the transmitter or be added as an external module. However, for short-distance communication, an extra amplifier may not be employed to reduce DC power consumption. The OOK receiver is generally composed of a THz pre-amplifier, a demodulator, and a baseband amplifier. The pre-amplifier and the baseband amplifier can be implemented in the form of on-chip integration or an external module. The OOK demodulation is realized commonly by a simple envelope detector.

B. Transistor Technology

The THz OOK transceivers chip sets are fabricated using a Teledyne 250-nm InP double-heterojunction bipolar transistor technology (DHBT) with the unity current gain frequency f_T of 350 GHz and the maximum oscillation frequency f_{MAX} of 650 GHz. The process offers four metal layers including 3 μm thick top metal and benzocyclobutene (BCB) with the relative permittivity $\varepsilon_r = 2.7$ as an inter-layer dielectric. Also, a thin film resistor with 50 Ω/sq and a metal-insulator-metal capacitor with 0.3 fF/μm^2 are provided.

C. Experimental Setup for Wireless Data Transmission

Fig. 1 shows a measurement setup for wireless data transmission of TRX1 and TRX2. A pseudorandom bit sequence (PRBS) generated by a Keysight M8195A arbitrary waveform generator (AWG) with a 65 Gsamples/s sampling rate is fed to the transmitter chip. The OOK modulated THz signal is radiated and received by WR-3.4 high-gain horn antennas with the frequency range of 220-325 GHz. The air channel distance d can be precisely adjusted from 3 cm to 25 cm by using a moving rail. The demodulated output of the receiver chip is measured by either a 1.5 Gbps Synthesys BitAlyzer1500 bit error rate tester (BERT) or a Tektronix DSA72004 real-time oscilloscope with 20 GHz bandwidth. The BERT provides the BER values directly without extraction steps from the measured data waveforms. Due to the limitation of the tester, the BER is measured by the BERT only for a data rate of 1.5 Gbps and below, while the BER for the data rate higher than 1.5 Gbps is calculated from the eye diagrams which are plotted by the oscilloscope, as will be described later. However, the number of the bits measured by the oscilloscope is limited by 10^6 at 1 Gbps, imposing a limit on the BER extraction. The results show small differences between the directly measured BER from the BERT and extracted BER from the oscilloscope waveforms.

IV. Transceiver Chip Set (TRX1)

In this section, we present the fabrication design of the first chip set (TRX1) which focuses on achieving a high on-chip integration level for short-range communication. We first explain the general architecture of the chip set and subsequently elaborate on each circuit block.

A. Architecture

The block diagrams of a transmitter and a receiver for TRX1 are shown in Fig. 2. The transmitter consists of a fundamental mode VCO for THz carrier generation and a passive switch for OOK modulation. The THz carrier frequency can be tuned from 272.4 GHz to 310.8 GHz by the VCO. Since the VCO is on-chip integrated in the transmitter, no additional blocks such as AMC and a low frequency source are needed for carrier generation. Furthermore, the fundamental VCO offers higher spectral purity of the carrier signal compared to harmonic-mode THz generators. The transmitter is targeted for short-distance communication and thus no amplifier is employed.

The receiver of TRX1 integrates a THz balun, a pre-amplifier, an envelope detector, a baseband active balun, and baseband amplifier in a single chip. To take an advantage of virtual ground and to suppress the common-mode noise, all the THz and baseband signal paths are designed in a differential topology. Thus, a THz balun and a baseband active balun are added before the THz pre-amplifier and the baseband amplifier, respectively. It is also noted that no additional baseband circuitry is externally needed for demodulation due to on-chip integration of baseband blocks.

B. Integrated THz OOK Transmitter

A high power wideband VCO is employed for on-chip carrier generation. A design of the THz fundamental mode VCO with sufficient output power is challenging because the transistor transconductance decreases significantly at the THz band. Fig. 3(a) shows the schematic and the chip micrograph of the VCO [42]. To fulfill the oscillation condition at the frequency above 270 GHz, a cascode cross-coupled

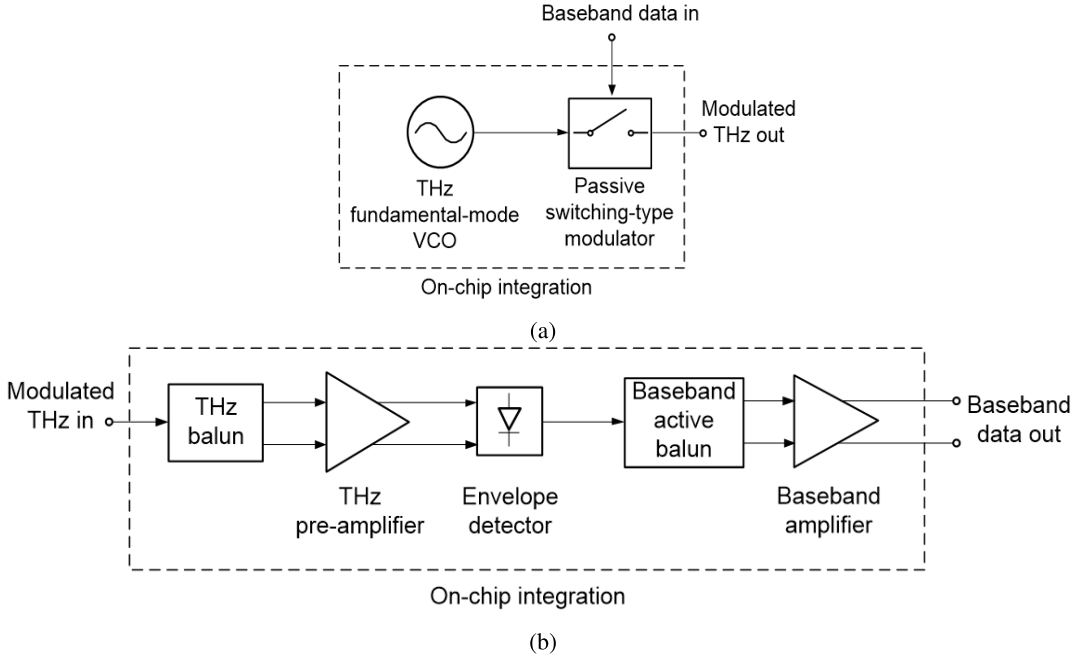

Fig. 2. Block diagrams of TRX1 (a) transmitter (b) receiver.

transistor pair is adopted for the oscillation core instead of a conventional common-emitter (CE) cross-coupled topology. Also, the emitters of the cross-coupled transistor pair are capacitively degenerated in order to obtain a wide frequency tuning range. With these techniques, the VCO exhibits high peak output power of 1.5 dBm at 272.4 GHz and a wide tuning range of 38.4 GHz from 272.4 GHz to 310.8 GHz. The measured phase noise at the 10 MHz offset is -96.4 dBc/Hz at 272.6 GHz.

For OOK modulation, a passive switching type modulator is designed. Compared to an active modulator, the passive modulator would be advantageous due to a wider bandwidth, lower DC power consumption, and higher linearity at the cost of a higher insertion loss. A triple-shunt transistor topology is employed to improve the isolation in the off-state. The measured insertion loss is lower than 3.5 dB and the isolation is higher than 14 dB in the entire WR-3.4 band from 220 GHz to 325 GHz.

Fig. 3(a) shows a full schematic and a chip micrograph of the transmitter, which integrates the VCO and the modulator as described previously. The chip occupies an area of 500×642 μm^2 including probing pads and consumes DC power of 226 mW. Fig. 3(b) exhibits the measured radio frequency (RF) performance of the transmitter. The carrier frequency is tuned from 272.4 GHz to 310.8 GHz and the peak carrier output power is -0.8 dBm at 274.3 GHz. The output power difference with the switch on and off is higher than 10 dB in the operation bandwidth, which is sufficiently high for the OOK modulation.

C. Integrated THz OOK Receiver

Fig. 4(a) presents the schematic of the THz pre-amplifier which consists of three cascaded gain cells. Each gain cell is based on a two stage differential common-base (CB) topology. A frequency staggered matching technique is used to achieve a wide bandwidth. Thus, three gain cells are designed such that they exhibit a peak gain at 290 GHz, 300 GHz, and 310 GHz, respectively. An L-section network provides 50 Ω matching at the input and output ports. A simulated noise figure is 14 dB at 300 GHz. The measured peak gain equals 19.1 dB at 299 GHz with a 3 dB bandwidth of 23 GHz from 285 GHz to 308 GHz.

An envelope detector is designed and fabricated for demodulation of the THz OOK signal to exploit its simple structure and low DC power consumption. The envelope detector employs a differential CE topology for high responsivity, high carrier rejection, and convenient integration with the preceding differential pre-amplifier as shown in Fig. 4(a). The simulated responsivity and the noise equivalent power (NEP) are measured to be 1.04 kV/W and 1.1 pW/$\sqrt{\text{Hz}}$, respectively, at 300 GHz when the input power is -40 dBm.

An on-chip baseband amplifier follows the envelope detector to boost the demodulated baseband signal. The baseband amplifier consists of two cascaded sets of a CE-EF (emitter-follower) chain. The first stage serves as an active balun which is required to convert a single ended output of the envelope detector into a differential signal. A remained input port of the first CE is terminated by a dummy envelope detector to improve the amplitude and the phase balance of the active balun. The second CE provides a voltage gain for the demodulated baseband signal. The EFs following the CEs serve as a DC level shifter and a 50 Ω matching buffer, respectively. The measured peak gain is 21 dB and a 10 dB bandwidth is equal to 38 GHz.

The chip micrograph of the integrated receiver in Fig. 4(a) occupies an area of 975×620 μm^2. In Fig. 4(b), we can see that the receiver achieves a high responsivity of 1400 kV/W

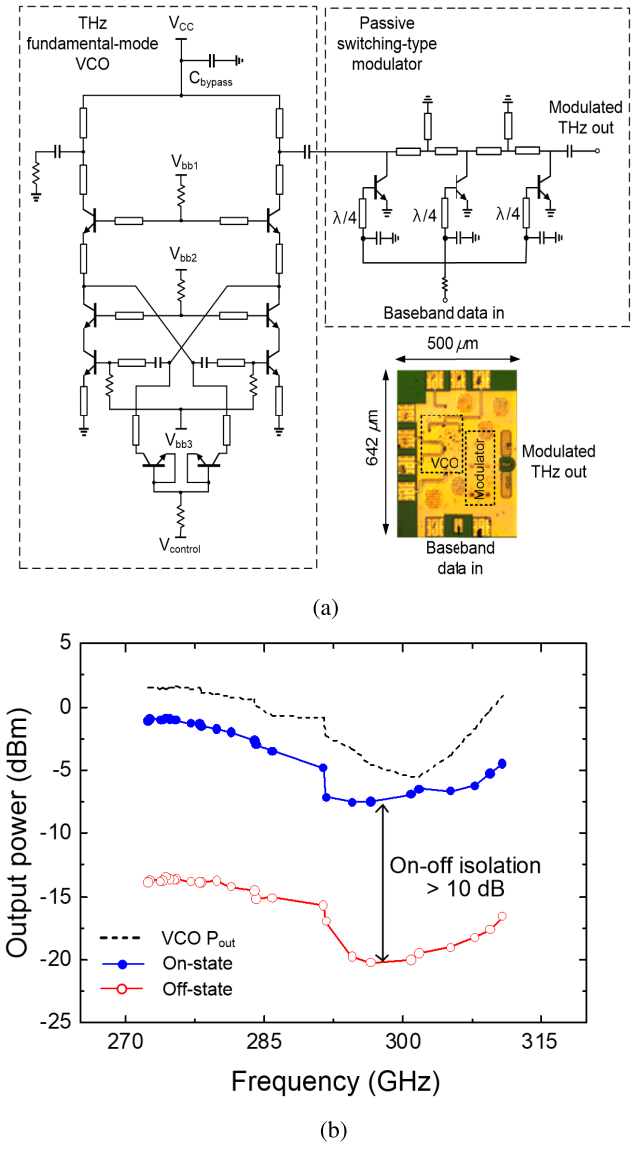

Fig. 3. (a) Schematic and chip micrograph (b) measured RF performance of TRX1 transmitter.

at 302 GHz, which is attributed to a high voltage gain originated from the integrated pre-amplifier and the baseband amplifier. A measured NEP maintains lower than 1.1 pW/$\sqrt{\text{Hz}}$ over a wide bandwidth from 278 GHz to 325 GHz. Thus, the wide bandwidth makes the chip suitable for wideband THz communication.

V. Transceiver Chipset (TRX2)

In this section, we present the fabrication design of the second chip set (TRX2) that focuses on providing higher transmit power by attaching amplifier waveguide modules to on-wafer transceiver circuits. We first explain the general architecture of this chip set and then present the details of different circuit modules.

A. Architecture

The link distance can be greatly extended by employing alternate versions of transmitter and receiver components for TRX2. These upgraded components deliver higher transmitted power with reduced internal losses. The transmitter block for TRX2 is constructed by adding an extra amplifier waveguide module to an integrated modulator circuit as shown in Fig. 5(a). While lacking an on-wafer local oscillator, the transmitter utilizes a Virginia Diodes Inc. (VDI) amplifier-multiplier-chain WR-3.4 AMC-I as an external THz source to conveniently tune the carrier frequency and power for an accurate OOK data link analysis. The modulator circuit consists of an amplifier-type switch followed by a milliwatt level output amplifier. The on-wafer modulator circuit requires a use of an RF probe with a substantial amount of insertion losses of up to 4 dB at 300 GHz to transmit the signal into the air through the 24-dBi RPG FH-PP-325 WR-3.4 corrugated circular horn antenna. The RF probe power loss could be overcome by inserting the amplifier module between the horn and the probe. The receiver block for TRX2 has the same amplifier module attached to the receiving horn antenna. The module is followed by another RF probe, an integrated demodulator circuit, and two commercial baseband amplifiers as shown in Fig. 5(b). The demodulator circuit includes a pre-stage amplifier and an envelope detector similar to the parts used in TRX1. The waveguide and the integrated amplifiers together should improve the system noise, and the external baseband amplifier ensures the final data voltage level to exceed the minimum detectable level of the oscilloscope. The external baseband amplifiers are SHF 100BP with a 17 dB gain from 20 kHz to 25 GHz and SHF 804M with 23 dB gain from 50 kHz to 65 GHz.

B. OOK Modulator

An amplifier-type switch proposed for the TRX2 modulator circuit provides a superior on-off ratio compared with a passive shunt switch for TRX1 due to a positive on-state amplifier gain and effective off-state isolation. The data signal is applied as the DC bias to the amplifier switch through the collector terminals of the transistors. The input data voltage levels are set to 1.8 V and 0 V for on and off states, respectively, to properly bias the amplifier switch. The amplifier switch has shortcomings of narrowed bandwidth due to the input and output matching networks and conceivably of larger group delay and data distortion from complex DC bias networks. A more detailed description of the single stage differential amplifier switch is provided in [43]. The output amplifier uses differential CB configuration for its unit cell design. An amplifier chain is formed by cascading four unit cell stages, and the final output amplifier subsequently combines power from four amplifier chains. More details of the output amplifier design are provided in [44]. The photograph and the small-signal static performance of the integrated modulator are illustrated in Fig. 6. The integrated modulator circuit has a peak gain of 12.3 dB and a 3 dB bandwidth of 32 GHz and provides better than 20 dB on-off ratio over 60 GHz bandwidth. The maximum on-state output power is measured as 7.4 dBm at 288 GHz.

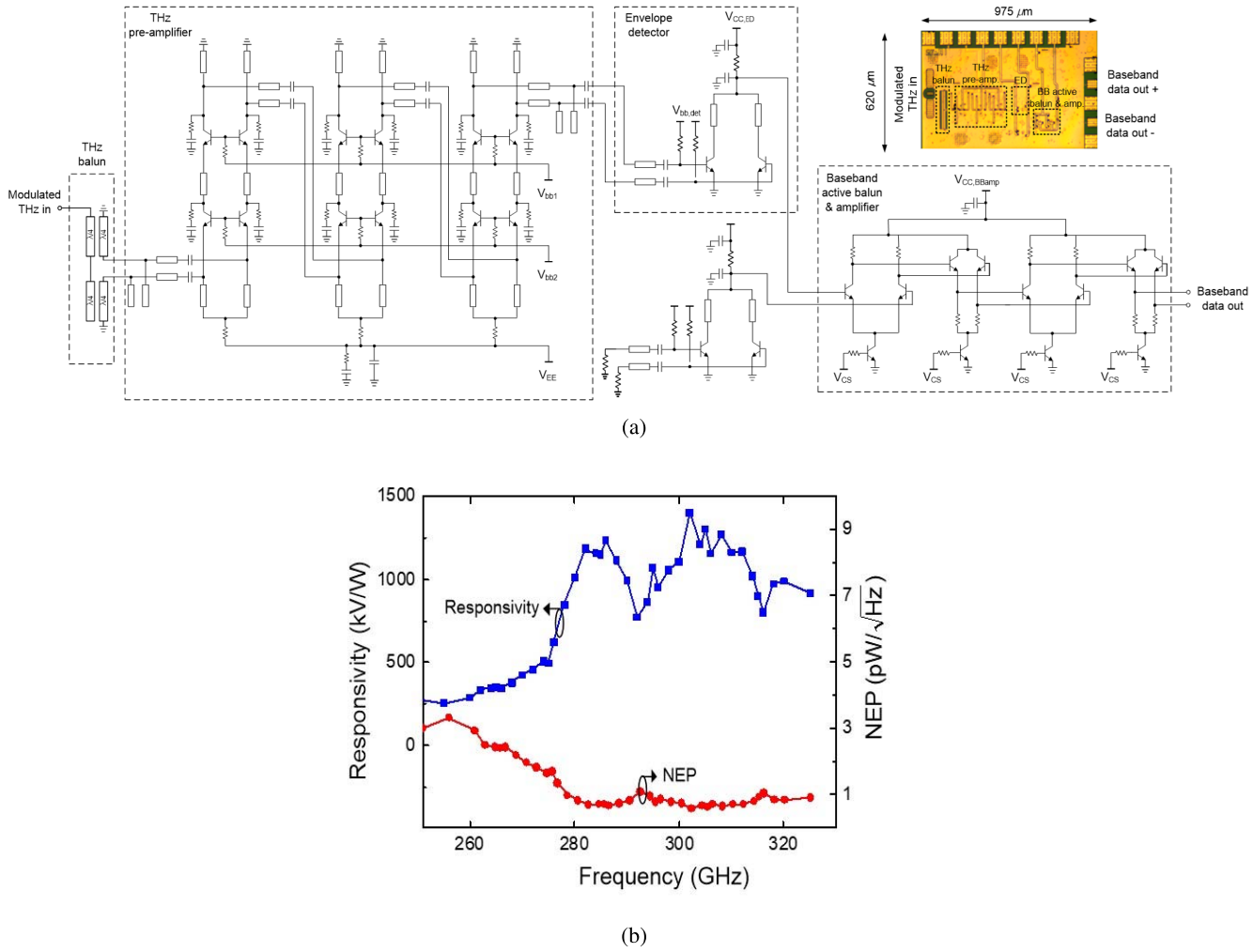

Fig. 4. (a) Schematic and chip micrograph (b) measured RF performance of the TRX1 receiver.

C. OOK Demodulator

The demodulator design for TRX2 does not differ significantly from the TRX1 design. The single chain four-stage pre-amplifier with the measured noise figure of 14 dB is expected to improve the receiver noise, and the envelope detector is almost identical to the design used in TRX1 except that a differential CB topology is employed instead of CE. A complete description of the integrated demodulator circuit containing a pre-amplifier and an envelope detector can be found in [45]. The chip photograph and the performance of the demodulator are presented in Fig. 7. The measurements on the integrated demodulator show the maximum responsivity of 1.28 kV/W and the minimum NEP of 0.31 pW/$\sqrt{\text{Hz}}$ at 302 GHz.

D. Amplifier Waveguide Module

The biggest difference between the two transceiver systems is two amplifier modules directly attached to the transmitting and receiving waveguide horn antennas for TRX2. Integrated amplifiers fabricated based on the same device technology are properly cut using a diamond sawing blade for waveguide packaging. These amplifiers contain low-loss waveguide-to-InP microstrip transitions so that the chip could be mounted directly without extra carrier substrates inside a standard WR-3.4 rectangular waveguide. A current amplifier design contains three separate amplifier chains and their respective miniaturized transitions for threefold increase in the power-handling capability. More details of the module design are provided in [46]. The assembled amplifier module provides more than 6.5 dBm of output power at 260 GHz. The layout of the amplifier chip and the photograph of the split waveguide blocks are shown in Fig. 8(a). Also, the small-signal performance of the amplifier module indicating the peak gain of 12.3 dB and a 3 dB bandwidth of 32 GHz is plotted in Fig. 8(b).

VI. Simulation Results

This section presents the numerical results based on the experimental observations for the proposed TRX1 and TRX2. Note that due to hardware limitations, obtaining the BER from the tester is not feasible for data rate higher than 1.5 Gbps. Moreover, the BER calculations from Monte Carlo simulations normally take long time because we need to adjust the alignment between the transmitted signal and the measured

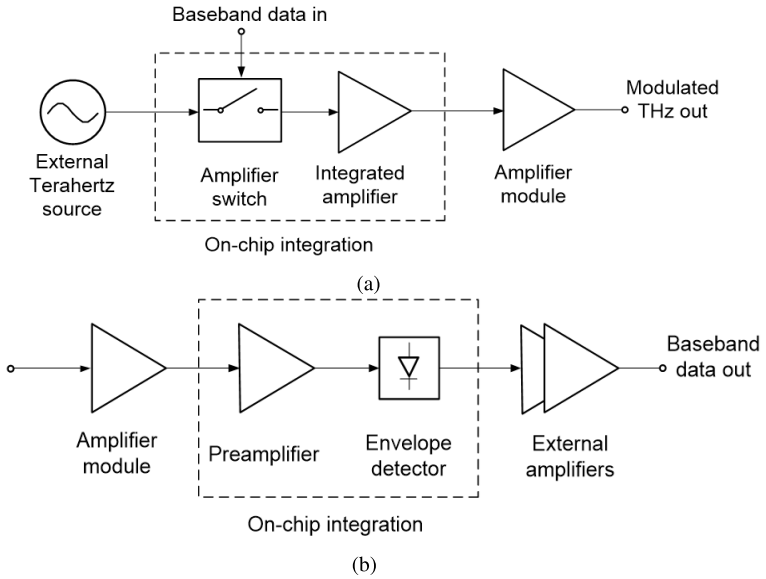

Fig. 5. Block diagrams of TRX2 (a) transmitter (b) receiver.

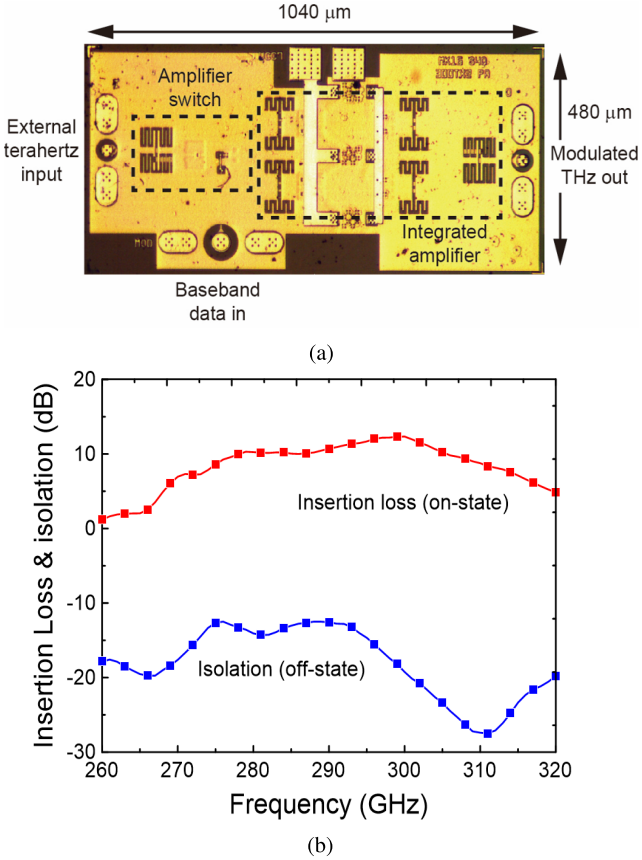

Fig. 6. (a) Chip photograph (b) measured insertion loss and isolation of the on-chip modulator of a transmitter in TRX2.

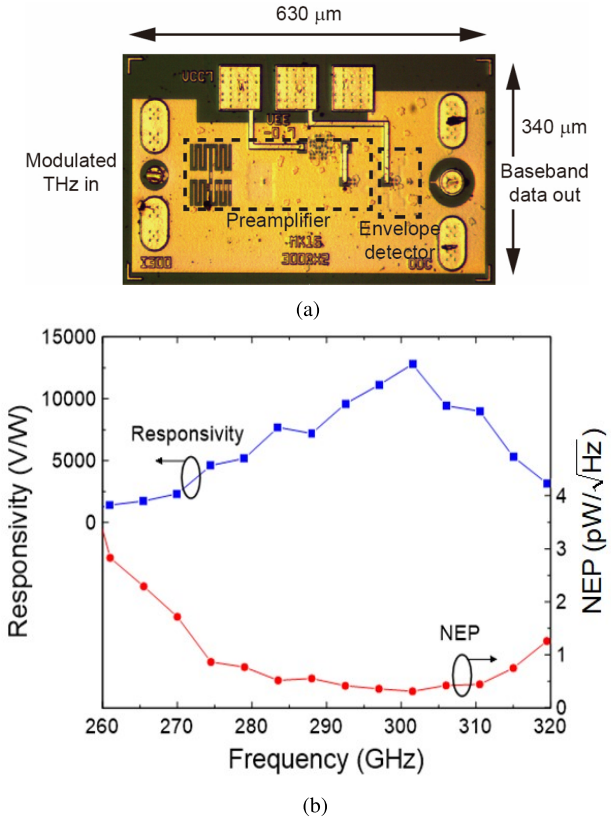

Fig. 7. (a) Chip photograph (b) measured responsivity and NEP of the on-chip demodulator of a receiver in TRX2.

received signal. Instead, to ensure a reliable BER estimate and allow simple computations, we compute the BER estimate based on an eye diagram by following the method described in [47], [48]. Furthermore, this approach has an the advantage of predicting a lower BER value regardless of the number of bits. After an eye diagram is obtained from the measurement data, an estimate of the SNR is calculated using the 40-60% region across the maximum eye opening instant. As such, the 40-60% region of the eye diagram constitutes all the data samples in the middle 20% of the eye period. Consequently, SNR can be given by $\text{SNR} = \left(\frac{\mu_1-\mu_0}{\sigma_1+\sigma_0}\right)^2$, where, μ_1, μ_0 and σ_1, σ_0 represent the mean and the standard deviation

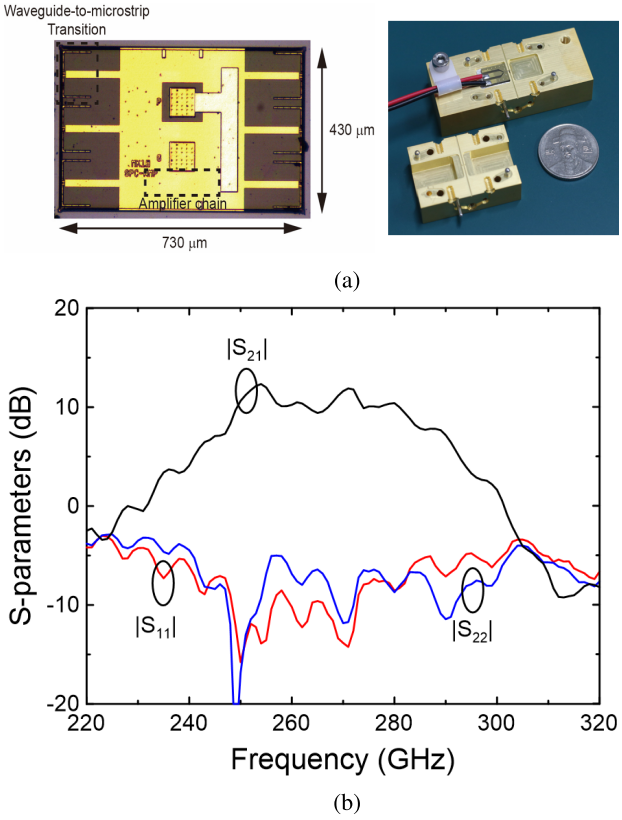

Fig. 8. (a) Photograph of the chip and the amplifier module (b) performance of the amplifier waveguide module.

of the histograms around on-state and off-state of the eye diagram, respectively. Then, the BER estimate is evaluated as $\text{BER} = \text{Q}\left(\sqrt{\text{SNR}}\right)$ where $\text{Q}(x)$ denotes the Q-function as $\text{Q}(x) = \int_x^\infty \frac{1}{\sqrt{2\pi}} \exp^{-\frac{y^2}{2}} dy$. It is emphasized that the description of various estimation methods for the BER in this paper is significantly distinct from the work in [49]. In what follows, we provide the BER results corresponding to both TRX1 and TRX2. Hereby, we analyze the impact of various parameters on the BER performance of the considered THz communications framework.

In Fig. 9, we present the BER performance of TRX2 in terms of the transmitted power with the data rate of 1 Gbps. It can be observed that the BER estimation from the eye diagram is fairly close to the BER tester results. Additionally, Monte Carlo simulations also corroborate the obtained BER results. It can be seen from the curves that the proposed transceiver design offers very low BER which makes it useful for practical applications. For instance, at $P_t = 0$ dBm, we obtain the BER of 10^{-8} at $d = 10$ cm with the estimated SNR of 14.8 dB. The BER will be further improved by increasing the transmit power. Also, we can check that comparing the BER tester results at $\text{BER} = 10^{-4}$, putting additional 5 dBm in the transmit power increases the distance from 10 cm to 15 cm.

In Fig. 10, we plot the BER performance against the transmission distance at the fixed power of 3 dBm and the data rate of 1 Gbps for both TRX1 and TRX2. From the curves, it can be witnessed that TRX2 supports a longer

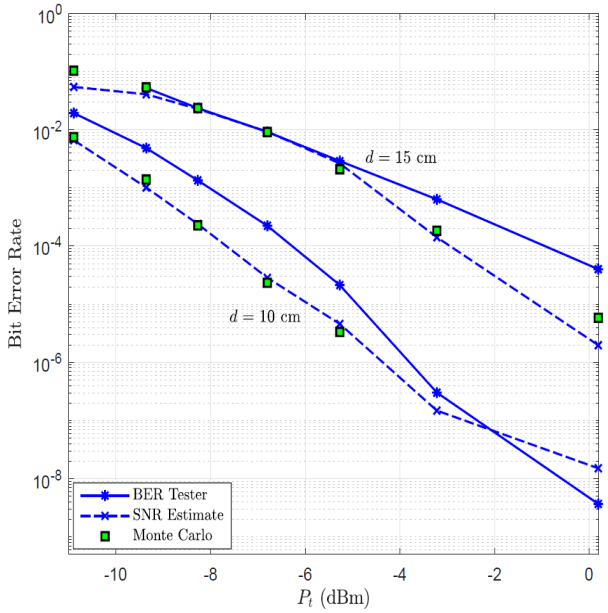

Fig. 9. BER in terms of the transmit power P_t for TRX2.

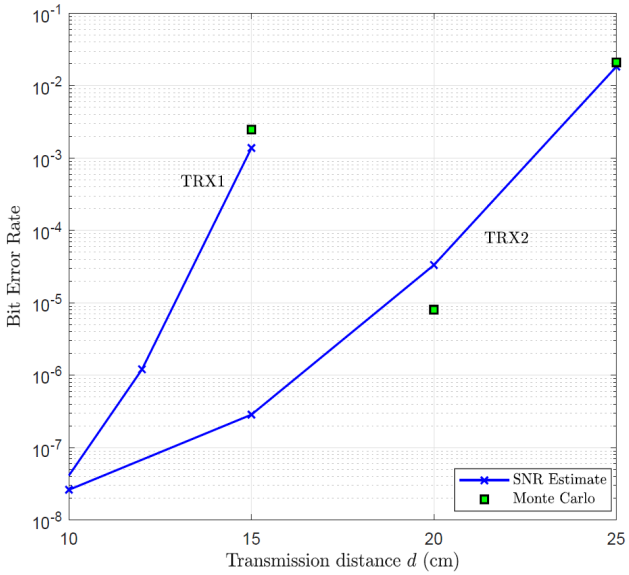

Fig. 10. BER in terms of the transmission distance d.

communication range for a given BER compared to TRX1 due to an inclusion of the THz amplifier waveguide module in a design of the chip set.[2] We can check that at $\text{BER} = 10^{-2}$ up to 25 cm distance can be supported with TRX2. If channel coding is adopted, the BER will be substantially decreased and, as a result, the distance can be further increased.

In Fig. 11, we examine the impact of the data rate on the BER performance at a fixed transmit power of 3 dBm. Again we can see that TRX2 offers better BER performance over

[2]For the performance of a shorter link distance of below 15 cm, our speculation is that due to power saturation of the receiver amplifier in TRX2 distorts the received data waveform and increases the BER. Signal distortion due to high received power for a shorter link distance has been observed in other transceiver systems [49].

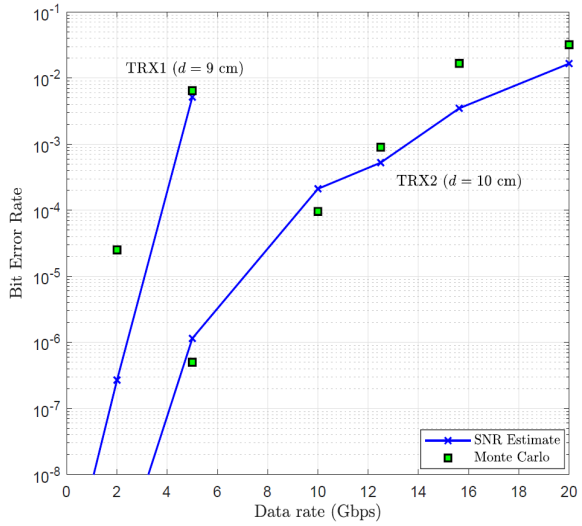

Fig. 11. BER in terms of the data rate.

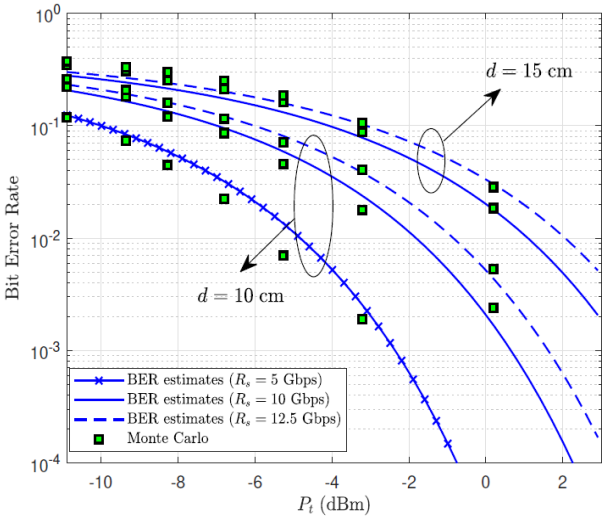

Fig. 13. BER in terms of the transmit power for different data rate and link distance.

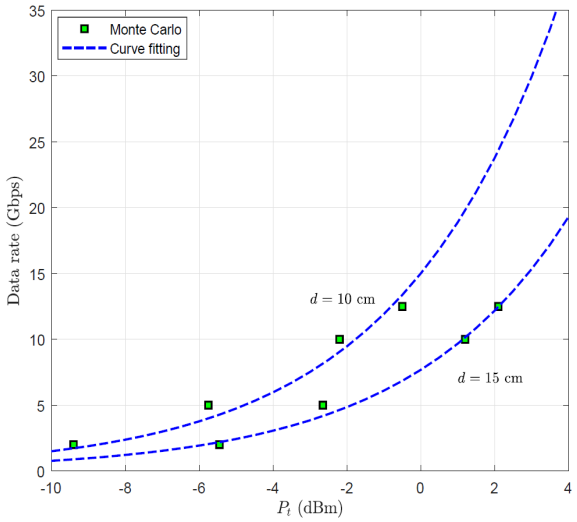

Fig. 12. Data rate in terms of the transmit power P_t for TRX2.

TRX1 even if the distance is longer. Also, we confirm that our BER computation based on the SNR estimate approach is accurate compared with the Monte Carlo results.

Fig. 12 demonstrates the behavior of the achievable data rate for TRX2 with respect to the transmit power at a fixed BER of 10^{-2}. For the case of $d = 10$ cm, the data rate of 10 Gbps is recorded at $P_t = -2.5$ dBm over a bandwidth of 10 GHz with the spectral efficiency of 1 bps/Hz. Further, a higher data rate can be achieved by exploiting abundant bandwidth available at THz frequencies and adopting higher transmit power. According to (5), we can realize that the data rate is linearly proportional to the transmit power when the BER is fixed, assuming that all the circuit components in the transceiver system possess unlimited frequency bandwidths and power capabilities. For WR-3.4, the bandwidth is given as 100 GHz, ranging from 220 GHz to 320 GHz. By applying the curve-fitting tools of MATLAB to the Monte Carlo simulated points, we can obtain $R_s = 1.84 P_{t[\mathrm{mW}]}/(\mathrm{SNR}\ d_{[\mathrm{m}]}^{1.65})$ Gbps in the form of (5). Note that the required SNR for the BER of 10^{-2} can be computed as 7.33 dB in the OOK system [50]. Based on this observation, we can check that the data rate of 1 Gbps is achievable at the distance of 1.6 m.

In Fig. 13, we finally present the BER performance of TRX2 against the transmit power to confirm the accuracy of our BER estimates for different data rate and transmission distance. In this case, the received SNR is computed by $\mathrm{SNR} = 1.84 P_{t[\mathrm{mW}]}/(R_s\ d_{[\mathrm{m}]}^{1.65})$ and the corresponding BER can be evaluated as $\mathrm{BER} = \mathrm{Q}\left(\sqrt{1.84 P_{t[\mathrm{mW}]}/(R_s\ d_{[\mathrm{m}]}^{1.65})}\right)$. It can be observed that our derived BER is quite close to the Monte Carlo results for various cases. Using this BER estimate, we are able to accurately predict the required transmit power for reliable THz communication with our chip set.

VII. Conclusion

In this work, we have designed and fabricated two THz OOK transceiver chip sets based on a 0.25 μm InP DHBT technology. The first transceiver chip set TRX1 integrates the circuit blocks for OOK modulation including an on-chip THz carrier source. By using external THz amplifier modules, the second chip set TRX2 successfully increases the transmit distance with better BER performance. In addition, we can further enhance the transmit distance by applying diversity techniques such as antenna arrays [52]. From the BER estimate, we can predict the BER performance as a function of transmission power and data rate for our proposed chip architecture.

Our work presented in this paper is just an early stage of THz communication implementation and we have demonstrated that high data rate links for beyond 5G systems are feasible by utilizing the proposed chip design techniques. Further improvements are possible by employing channel coding, high level constellation, and multiple-input and multiple-output (MIMO) techniques [53]–[55].

REFERENCES

[1] C. Yi *et al.*, "THz wireless systems design for personal area networks applications," in *Proc. Int. Conf. ICT Converg. (ICTC)*, Oct. 2020, pp. 529–531.

[2] S. Cherry, "Edholm's law of bandwidth," *IEEE Spectr.*, vol. 41, no. 7, pp. 58–60, Jul. 2004.

[3] Ericsson. (Jun. 2020). *Mobile Data Traffic Outlook, Mobility Report*. [Online]. Available: https://www.ericsson.com/en/mobility-report/dataforecasts/mobile-traffic-forecast

[4] T. S. Rappaport *et al.*, "Wireless communications and applications above 100 GHz: Opportunities and challenges for 6G and beyond," *IEEE Access*, vol. 7, pp. 78729–78757, 2019.

[5] P. Chatzimisios, D. Soldani, A. Jamalipour, A. Manzalini, and S. K. Das, "Special issue on 6G wireless systems," *J. Commun. Netw.*, vol. 22, no. 6, pp. 440–443, Dec. 2020.

[6] *IEEE 802.15 WPAN Terahertz Interest Group (IGthz)*. Accessed: Jul. 23, 2014. [Online]. Available: http://www.ieee802.org/15/pub/TG3d/index_IGthz.html

[7] I. F. Akyildiz, J. M. Jornet, and C. Han, "Terahertz band: Next frontier for wireless communications," *Phys. Commun.*, vol. 12, p. 16–32, Sep. 2014.

[8] J. Pang *et al.*, "A 50.1-Gb/s 60-GHz CMOS transceiver for IEEE 802.11ay with calibration of LO feedthrough and I/Q imbalance," *IEEE J. Solid-State Circuits*, vol. 54, no. 5, pp. 1375–1390, May 2019.

[9] J. Pang *et al.*, "A 28-GHz CMOS phased-array beamformer utilizing neutralized bi-directional technique supporting dual-polarized MIMO for 5G NR," *IEEE J. Solid-State Circuits*, vol. 55, no. 9, pp. 2371–2386, Sep. 2020.

[10] Y. Wang *et al.*, "A 60-GHz 3.0-Gb/s spectrum efficient BPOOK transceiver for low-power short-range wireless in 65-nm CMOS," *IEEE J. Solid-State Circuits*, vol. 54, no. 5, pp. 1363–1374, May 2019.

[11] H. Kaushal and G. Kaddoum, "Optical communication in space: Challenges and mitigation techniques," *IEEE Commun. Surveys Tuts.*, vol. 19, no. 1, pp. 57–96, 1st Quart., 2017.

[12] T. Koonen, "Indoor optical wireless systems: Technology, trends, and applications," *J. Lightw. Technol.*, vol. 36, no. 8, pp. 1459–1467, Apr. 15, 2018.

[13] H. Elayan, O. Amin, B. Shihada, R. M. Shubair, and M.-S. Alouini, "Terahertz band: The last piece of RF spectrum puzzle for communication systems," *IEEE Open J. Commun. Soc.*, vol. 1, pp. 1–32, 2019.

[14] O. Alkhazragi *et al.*, "7.4-Gbit/s visible-light communication utilizing wavelength-selective semipolar micro-photodetector," *IEEE Photon. Technol. Lett.*, vol. 32, no. 13, pp. 767–770, Jul. 1, 2020.

[15] Y. Yang, J. Luo, C. Chen, Z. Chen, W.-D. Zhong, and L. Chen, "Pushing the data rate of practical VLC via combinatorial light emission," *IEEE Trans. Mobile Comput.*, vol. 20, no. 5, pp. 1979–1992, Feb. 2020.

[16] A. Hirata *et al.*, "10-Gbit/s wireless link using InP HEMT MMICs for generating 120-GHz-band millimeter-wave signal," *IEEE Trans. Microw. Theory Techn.*, vol. 57, no. 5, pp. 1102–1109, May 2009.

[17] A. Hirata *et al.*, "120-GHz-band wireless link technologies for outdoor 10-Gbit/s data transmission," *IEEE Trans. Microw. Theory Techn.*, vol. 60, no. 3, pp. 881–895, Mar. 2012.

[18] K. Guan *et al.*, "Measurement, simulation, and characterization of train-to-infrastructure inside-station channel at the terahertz band," *IEEE Trans. THz Sci. Technol.*, vol. 9, no. 3, pp. 291–306, May 2019.

[19] K. Guan *et al.*, "Channel characterization for intra-wagon communication at 60 GHz and 300 GHz bands," *IEEE Trans. Veh. Technol.*, vol. 68, no. 6, pp. 5193–5207, Jun. 2019.

[20] S. Priebe and T. Kurner, "Stochastic modeling of THz indoor radio channels," *IEEE Trans. Wireless Commun.*, vol. 12, no. 9, pp. 4445–4455, Aug. 2013.

[21] C. Han, A. O. Bicen, and I. F. Akyildiz, "Multi-ray channel modeling and wideband characterization for wireless communications in the terahertz band," *IEEE Trans. Wireless Commun.*, vol. 14, no. 5, pp. 2402–2412, May 2015.

[22] S. Kim and A. Zajić, "Statistical modeling and simulation of short-range device-to-device communication channels at sub-THz frequencies," *IEEE Trans. Wireless Commun.*, vol. 15, no. 9, pp. 6423–6433, Sep. 2016.

[23] J. M. Jornet and I. F. Akyildiz, "Channel modeling and capacity analysis for electromagnetic wireless nanonetworks in the terahertz band," *IEEE Trans. Wireless Commun.*, vol. 10, no. 10, pp. 3211–3221, Oct. 2011.

[24] J. Kokkoniemi, J. Lehtomäki, K. Umebayashi, and M. Juntti, "Frequency and time domain channel models for nanonetworks in terahertz band," *IEEE Trans. Antennas Propag.*, vol. 63, no. 2, pp. 678–691, Feb. 2015.

[25] C.-C. Wang, X.-W. Yao, C. Han, and W.-L. Wang, "Interference and coverage analysis for terahertz band communication in nanonetworks," in *Proc. IEEE Glob. Commun. Conf.*, Singapore, Dec. 2017, pp. 1–6.

[26] J. M. Jornet and I. F. Akyildiz, "Graphene-based plasmonic nanoantenna for terahertz band communication," *IEEE J. Sel. Areas Commun.*, vol. 31, no. 12, pp. 685–694, Dec. 2013.

[27] T. Nagatsuma, G. Ducournau, and C. C. Renaud, "Advances in terahertz communications accelerated by photonics," *Nature Photon.*, vol. 10, pp. 371–379, May 2016.

[28] I. Mehdi, J. V. Siles, C. Lee, and E. Schlecht, "THz diode technology: Status, prospects, and applications," *Proc. IEEE*, vol. 105, no. 6, pp. 990–1007, Jun. 2017.

[29] M. Urteaga, Z. Griffith, M. Seo, J. Hacker, and M. J. W. Rodwell, "InP HBT technologies for THz integrated circuits," *Proc. IEEE*, vol. 105, no. 6, pp. 1051–1067, Jun. 2017.

[30] K. Sengupta, T. Nagatsuma, and M. D. Mittleman, "Terahertz integrated electronic and hybrid electronic-photonic systems," *Nature Electron.*, vol. 1, pp. 622–635, Dec. 2018.

[31] J.-D. Park, S. Kang, S. V. Thyagarajan, E. Alon, and A. M. Niknejad, "A 260 GHz fully integrated CMOS transceiver for wireless chip-to-chip communication," in *IEEE Symp. VLSI Circuits Dig.*, Jun. 2012, pp. 48–49.

[32] S. Moghadami, F. Hajilou, P. Agrawal, and S. Ardalan, "A 210 GHz fully-integrated OOK transceiver for short-range wireless chip-to-chip communication in 40 nm CMOS technology," *IEEE Trans. THz Sci. Technol.*, vol. 5, no. 5, pp. 737–741, Sep. 2015.

[33] Z. Wang, P.-Y. Chiang, P. Nazari, C.-C. Wang, Z. Chen, and P. Heydari, "A CMOS 210 GHz fundamental transceiver with OOK modulation," *IEEE J. Solid-State Circuits*, vol. 49, no. 3, pp. 564–580, Mar. 2014.

[34] Z. Chen *et al.*, "A survey on terahertz communications," *China Commun.*, vol. 16, no. 2, pp. 1–35, Feb. 2019.

[35] X. Timoneda *et al.*, "Engineer the channel and adapt to it: Enabling wireless intra-chip communication," *IEEE Trans. Commun.*, vol. 68, no. 5, pp. 3247–3258, May 2020.

[36] IEEE P802.15 Working Group for Wireless Personal Area Networks (WPANs). (Nov. 2016). *Proposal for IEEE 802.15.3D S THz PHY*. [Online]. Available: https://mentor.ieee.org/802.15/documents?is_group=003d&n=2

[37] A.-A. A. Boulogeorgos *et al.*, "Performance evaluation of THz wireless systems operating in 275-400 GHz band," in *Proc. IEEE Veh. Technol. Conf. (VTC)*, Porto, Portugal, Jun. 2018, pp. 1–5.

[38] *Recommendation, Attenuation by Atmospheric Gases and Related Effects*, document ITU-R P.676-11, 2008. [Online] https://www.itu.int/rec/R-REC-P.676

[39] S. Sun, G. R. MacCartney, and T. S. Rappaport, "Millimeter-wave distance-dependent large-scale propagation measurements and path loss models for outdoor and indoor 5G system,"'in *Proc. 10th Eur. Conf. Antennas Propag.*, Cham, Switzerland, pp. 1–5, Apr. 2016.

[40] S. Kim and A. G. Zajić, "Statistical characterization of 300-GHz propagation on a desktop," *IEEE Trans. Veh. Technol.*, vol. 64, no. 8, pp. 3330–3338, Aug. 2015.

[41] G. L. Stüber, *Principles of Mobile Communication*, 2nd ed. Norwell, MA, USA: Kluwer, 2001.

[42] D. Kim and S. Jeon, "A WR-3 band fundamental voltage-controlled oscillator with a wide frequency tuning range and high output power," *IEEE Trans. Microw. Theory Techn.*, vol. 67, no. 7, pp. 2759–2768, Jul. 2019.

[43] C. Yi, S. H. Choi, M. Urteaga, and M. Kim, "20-Gb/s on-off-keying modulators using 0.25-μm InP DHBT switches at 290 GHz," *EEE Microw. Wireless Compon. Lett.*, vol. 29, no. 5, pp. 360–362, May 2019.

[44] H. G. Yu, S. H. Choi, S. Jeon, and M. Kim, "300 GHz InP HBT amplifier with 10 mW output power," *Electron. Lett.*, vol. 50, no. 5, pp. 377–379, Feb. 2014.

[45] C. Yi, M. Urteaga, S. H. Choi, and M. Kim, "A 280-GHz InP DHBT receiver detector containing a differential preamplifier," *IEEE Trans. THz Sci. Technol.*, vol. 7, no. 2, pp. 209–217, Mar. 2017.

[46] C. Yi, J. Cho, J. Shin, and M. Kim, "260-GHz waveguide module containing an integrated InP HBT amplifier chip," *IET Electron. Lett.*, vol. 56, no. 13, pp. 665–667, Jun. 2020.

[47] *Eye Measurement Probe*. Accessed: Aug. 17, 2009. [Online]. Available: https://edadocs.software.keysight.com/display/ads2009U1/Eye+Probe

[48] W. Freude *et al.*, "Quality metrics for optical signals: Eye diagram, Q-factor, OSNR, EVM and BER," in *Proc. 14th Int. Conf. Transparent Opt. Netw. (ICTON)*, Jul. 2012, pp. 1–4.

[49] H. Song, "Demonstration of 20-Gbps wireless data transmission at 300 GHz for KIOSK instant data downloading applications with InP MMICs," *IEEE MTT-S Int. Microw. Symp. Dig.*, San Francisco, CA, May 2016, pp. 1–4.

[50] A. Goldsmith, *Wireless Communication*. Cambridge, U.K.: Cambridge Univ. Press, 2005.

[51] J. Rollin, D. Miller, M. Urteaga, Z. M. Griffith, and H. Kazemi, "A polystrata 820 mW G-band solid state power amplifier," in *Proc. IEEE Compound Semiconductor Integr. Circuit Symp. (CSICS)*, New Orleans, LA, USA, Oct. 2015, pp. 1–4.

[52] C. Lin and G. Y. Li, "Indoor terahertz communications: How many antenna arrays are needed?" *IEEE Trans. Wireless Commun.*, vol. 14, no. 6, pp. 3097–3107, Jun. 2015.
[53] J. Kim, H. Lee, C. Song, T. Oh, and I. Lee, "Sum throughput maximization for multi-user MIMO cognitive wireless powered communication networks," *IEEE Trans. Wireless Commun.*, vol. 16, no. 2, pp. 913–923, Feb. 2017.
[54] Z. Zhu, Z. Chu, N. Wang, S. Huang, Z. Wang, and I. Lee, "Beamforming and power splitting designs for AN-aided secure multi-user MIMO SWIPT systems," *IEEE Trans. Inf. Forensics Security*, vol. 12, no. 12, pp. 2861–2874, Dec. 2017.
[55] N. K. D. Venkategowda, H. Lee, and I. Lee, "Joint transceiver designs for MSE minimization in MIMO wireless powered sensor networks," *IEEE Trans. Wireless Commun.*, vol. 17, no. 8, pp. 5120–5131, Aug. 2018.

Changhwan Yi received the B.S. and Ph.D. degrees from the School of Electrical Engineering, Korea University, Seoul, South Korea, in 2015 and 2021, respectively. He is currently a Research Professor with the Terahertz Laboratory, Korea University. His current research interests include TMIC design, wireless communication systems, waveguide packaging, and spatial power-combining technique in terahertz frequency. He was a recipient of the Best Paper Award at the International Conference on ICT Convergence (ICTC), Jeju Island, South Korea, in October 2020.

Dongkyo Kim (Graduate Student Member, IEEE) received the B.S. and Ph.D. degrees in electrical engineering from Korea University, Seoul, South Korea, in 2015 and 2021, respectively. He is currently with Samsung Electronics, Suwon, South Korea. His research interests include mm-wave and terahertz integrated circuits and transceiver systems for communication applications.

Sourabh Solanki (Member, IEEE) received the M.Tech. degree in communication and signal processing and the Ph.D. degree in electrical engineering from the Indian Institute of Technology Indore (IIT Indore), India, in 2015 and 2019, respectively. From 2019 to 2020, he was a Research Professor with the Korea University, Seoul, South Korea, where he received the Brain Korea 21 Postdoctoral Fellowship by the National Research Foundation, Government of Korea. He is currently working as a Research Associate with the Interdisciplinary Centre for Security, Reliability and Trust (SnT), University of Luxembourg, Luxembourg. His main research interests include cognitive radio, terahertz communications, mmWave networks, energy harvesting, and unmanned aerial vehicle (UAV)-based wireless systems. He has been serving as a technical program committee member of various conferences and has also been involved in peer review process of major IEEE journals and conferences. He is a member of IEEE Communications Society. He was a co-recipient of the Best Paper Award at the International Conference on ICT Convergence (ICTC), Jeju Island, South Korea, in October 2020.

Jae-Hong Kwon (Member, IEEE) received the B.S. degree in electrical engineering from Korea University, Seoul, South Korea, in 2014. He is currently pursuing the Ph.D. degree with the School of Electrical Engineering, Korea University. His research interests include energy efficiency of communication systems, millimeter wave communications, and beamforming techniques.

Moonil Kim (Senior Member, IEEE) received the Ph.D. degree from the California Institute of Technology, Pasadena, CA, USA, in 1993. He has been a member of the Faculty of Electrical Engineering, Korea University, Seoul, South Korea, since 2000. He was a member of Technical Staff with the Submillimeter-Wave Advanced Technology Group, Jet Propulsion Laboratory, until 1998, and a Senior Scientist with the Microwave Group, Rockwell Science Center (currently Teledyne Scientific) until 2000. His current research interests include development of both passive and active circuit components required in construction of terahertz communication and imaging systems.

Sanggeun Jeon (Member, IEEE) received the B.S. and M.S. degrees in electrical engineering from Seoul National University, Seoul, South Korea, in 1997 and 1999, respectively, and the M.S. and Ph.D. degrees in electrical engineering from the California Institute of Technology (Caltech), Pasadena, CA, USA, in 2004 and 2006, respectively. From 1999 to 2002, he was a full-time Instructor in electronics engineering at the Korea Air Force Academy, Cheongju, South Korea, where he was a Research Engineer from 2006 to 2008; involved in CMOS phased-array receiver design. Since 2008, he has been with the School of Electrical Engineering, Korea University, Seoul, South Korea, where he is currently a Professor. His current research interests include integrated circuits and systems at microwave, millimeter-wave, and terahertz bands for high-speed wireless communications and high-resolution imaging applications.

Young-Chai Ko (Senior Member, IEEE) received the B.Sc. degree in electrical and telecommunication engineering from Hanyang University, Seoul, South Korea, and the M.S.E.E. and Ph.D. degrees in electrical engineering from the University of Minnesota, Minneapolis, MN, USA, in 1999 and 2001, respectively. In 2001, he was with Novatel Wireless as a Research Scientist. In 2001, he joined the Wireless Center, Texas Instruments Incorporated, San Diego, CA, USA, as a Senior Engineer. He is currently a Professor with the School of Electrical Engineering, Korea University. His current research interests include the performance analysis and the design of wireless communication systems.

Inkyu Lee (Fellow, IEEE) received the B.S. degree (Hons.) in control and instrumentation engineering from Seoul National University, Seoul, South Korea, in 1990, and the M.S. and Ph.D. degrees in electrical engineering from Stanford University, Stanford, CA, USA, in 1992 and 1995, respectively. From 1995 to 2002, he was a member of the Technical Staff with Bell Laboratories, Lucent Technologies, Murray Hill, NJ, USA, where he studied high-speed wireless system designs. Since 2002, he has been with Korea University, Seoul, where he is currently a Professor with the School of Electrical Engineering. He has also served as the Department Head for the School of Electrical Engineering, Korea University, from 2019 to 2021. In 2009, he was a Visiting Professor with the University of Southern California, Los Angeles, CA, USA. He has authored or coauthored more than 190 journal articles in IEEE publications and holds 30 U.S. patents granted or pending. His research interests include digital communications, signal processing, and coding techniques applied for next-generation wireless systems. Dr. Lee was a recipient of the IT Young Engineer Award at the IEEE/IEEK Joint Award in 2006, the Best Paper Award at the Asia–Pacific Conference on Communications in 2006, the IEEE Vehicular Technology Conference in 2009, the IEEE International Symposium on Intelligent Signal Processing and Communication Systems in 2013, the Best Research Award from the Korean Institute of Communications and Information Sciences in 2011, the Best Young Engineer Award from the National Academy of Engineering of Korea in 2013, and the Korea Engineering Award from the National Research Foundation of Korea in 2017. He has served as an Associate Editor for the IEEE TRANSACTIONS ON COMMUNICATIONS from 2001 to 2011 and the IEEE TRANSACTIONS ON WIRELESS COMMUNICATIONS from 2007 to 2011. In addition, he was a Chief Guest Editor for the IEEE JOURNAL ON SELECTED AREAS IN COMMUNICATIONS (Special Issue on 4G Wireless Systems) in 2006. He currently serves as the Co-Editor-in-Chief for the *Journal of Communications and Networks*. He has been elected as a member of the National Academy of Engineering of Korea in 2015, and is currently a Distinguished Lecturer of IEEE.